Chapter

Methodology for Abrasive Wear Evaluation in Elevator Stage Centrifugal Pump Impellers

Rodrigo O.P. Serrano, José G. do V. Moreira, Ana L.P. de Castro, Maria A. Pinto, Edna M. de F. Viana and Carlos B. Martinez

Abstract

The abrasion resistance of the impellers depends on the characteristics of the materials used in their manufacture. In this work, a methodology is proposed for the evaluation of the abrasive wear of the plates of the centrifugal pump impellers, used in the gross water infrastructure station (GWIS) of sedimentary rivers, due to the sediment load variation and the river fluviometric dimension. In order to determine the wear mode and the relationship of the material-specific wear coefficient (K), due to the sediment concentration, a rotating ball abrasometer test was performed on SAE 8620, gray cast iron (GCI), and nodular cast iron (NCI), used in the manufacture of impellers. As an abrasive suspension, the concentrations of 1, 2, 3, 5, and 10 g L^{-1} of sediment were used in distilled water. The wear volume as a function of the relative velocity of the mixture in relation to the impeller blades was estimated mathematically. The results show that: i) The abrasive capacity of the sediments in different concentrations; ii) SAE 8620 steel was more resistant to abrasive wear; and iii) the rotational control of the pump as a function of sediment concentration and river level showed the possibility of reducing wear by 30%.

Keywords: abrasive wear, microabrasion, sediment concentration, hydroabrasion, pumping system

1. Introduction

Gross water elevation stations (GWES), installed in rivers of sedimentary basins, suffer from impeller wear due to the abrasive drag of the sediment load that descends through rivers throughout the year. To understand this process, we analyzed the abrasive wear caused by the sediments in three metal alloys used in the manufacture of centrifugal pump impellers for QWES.

In this study, the sediment concentration variation from 38 to 840 mg L^{-1} of Acre River was considered [1]. In recent work, in which the particle size of the particles pumped by GWES was analyzed, a higher concentration of particles was found between 50 and 100 μm [2].

The abrasive effects of the sediments may cause furrows on the surfaces of the impellers due to the impact of the particles, increasing the distortion of the grooves due to the increase of the particle diameter [3].

In view of these issues, it was necessary to study the regions of greatest vulnerability to wear, as well as to analyze the evolution of the wear, due to the variation of the sediment concentration at the time, the speed of rotation, variation of the head (ΔH) and of the material used in the manufacture of the rotors.

2. Abrasive wear mechanism

The mechanisms of abrasive wear are part of the tribological studies that study the interactions of surfaces in relative movement [4]. Such interaction takes into account friction, wear, and lubrication, in view of the economic, scientific, and technological interest in minimizing wear and tear (**Figure 1**).

The relationship of friction and wear will depend on the properties and shape of the surface of the material, as well as on the characteristics of the abrasive agent such as the size, shape, and hardness of the particles [5].

According to ASTM G40 [6], wear is the progressive loss of matter from the surface of a solid body due to contact and relative movement with another solid, liquid, or gaseous body. The standard DIN 50320 [7] presents a similar definition and highlights four types of wear mechanisms, among which the abrasive wear (**Figure 2**).

The abrasive wear volume can be calculated by the equation given by Archard and Hirst [8], which is directly proportional to the normal load and the relative

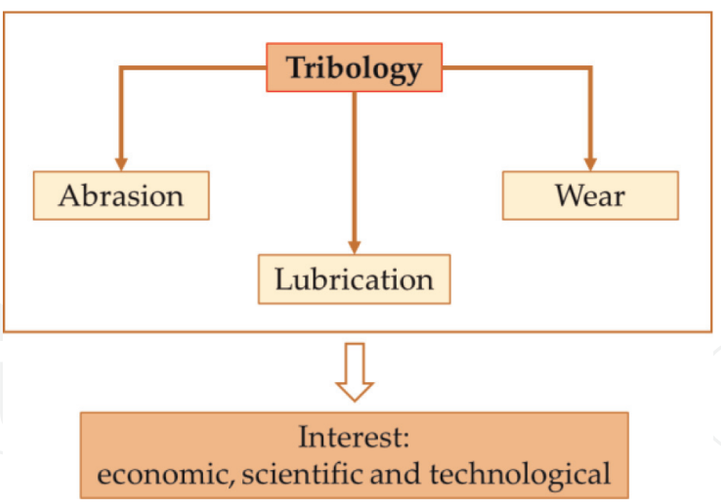

Figure 1.
Flowchart of the interaction of abrasion, wear, and lubrication in the tribological study.

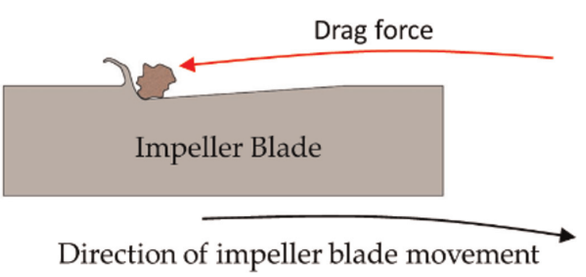

Figure 2.
Mechanism of abrasive wear on impeller blades of centrifugal pumps.

movement distance and inversely proportional to the hardness of the material (Eq. 1).

$$Vw = \frac{k}{\mathrm{Hm}} \bullet FN \bullet S \tag{1}$$

Wear can also be determined by trials in tribosystems, where parameters such as surface properties, chemical composition of the material, slip distance, velocity, and applied load are considered for a better understanding of the wear mechanisms [9, 10].

In pumping systems, wear is the result of the friction that occurs between the continuous water stream and the surface of the impeller blades, in a purely mechanical process [11], classified as hydroabrasive wear.

On the surface of the impeller blades, the microcut can occur due to the multiple impacts of the abrasive particles, being evident that the surface wear intensity depends mainly on the kinetic energy of the particles carried by the flow [12].

3. Methodology

Considering that there are several manufacturers and models of pumps that can work in GWES and the difficulties of acquiring the projects of the appropriate manufacturers, it was decided to carry out this study based on a project impeller. In order to do so, the algorithms developed by Palomino [13], which correlate the main design characteristics of a centrifugal pump impeller, as a function of flow rate (Q), manometric height (H), and rotation of the motor pump system, that is, as a function of the specific rotation (nq), given by Eq. (2).

$$nq = 3.65\frac{n\sqrt{Q}}{H^{3/4}} \tag{2}$$

This algorithm takes into account the sequence proposed in Chapters 4–6, 8, and 10–12 of the book by Macintyre [14], allowing for a quick determination of an impeller designs (Eq. 3–29).

$$\text{Estimate of hydraulic yield } (\varepsilon),\ \varepsilon = 1 - \frac{0.8}{\sqrt[4]{Q_{gpm}}} \tag{3}$$

$$\text{Driving power } (N_{cv}),\ N_{cv} = \frac{1000\ QH}{75\eta_t} \tag{4}$$

$$\text{Shaft diameter } (dei),\ dei = 12\sqrt[3]{\frac{N_{cv}}{n}} \tag{5}$$

$$\text{Shaft diameter—corrected } (dei_{corr}),\ dei_{corr} = 1.15(dei) \tag{6}$$

$$\text{Core diameter } (dn),\ dn = dei_{corr} + (2\ (5 \text{ to } 15\ mm)) \tag{7}$$

$$\text{Average speed at the impeller inlet } (v'_1),\ v'_1 = kv'_1\sqrt{2gH} \tag{8}$$

$$\text{Diameter of the impeller inlet port } (d'_1),\ d'_1 = \sqrt{\frac{4Q'}{\pi v'_1} + (dn)^2} \tag{9}$$

$$\text{Southern speed at impeller inlet } (v_{m1}),\ v_{m1} = k_{vm1}\sqrt{2gH} \tag{10}$$

$$\text{Peripheral speed at the leading edge } (u_1),\ u_1 = \frac{\pi d_{m1} n}{60} \tag{11}$$

$$\text{Shovel inclination angle } \beta_1 \text{ at the impeller inlet, } \tan\beta_1 = \frac{v_{m1}}{u_1} \quad (12)$$

$$\text{Number of blades } (Z),\ Z = 6,5\left(\frac{d_2 + d_{m1}}{d_2 - d_{m1}}\right) sen\left(\frac{\beta_1 + \beta_2}{2}\right) \quad (13)$$

$$\text{Circumferential pitch between the blades at the impeller inlet } (t_1),\ t_1 = \frac{\pi d_{m1}}{Z} \quad (14)$$

$$\text{Obstruction due to the blade thickness at the impeller inlet } (\sigma),\ \sigma_1 = \frac{S_1}{Sen\beta_1} \quad (15)$$

$$\text{Coefficient of contraction } (\gamma_1),\ \frac{1}{\gamma_1} = \frac{t_1}{t_1 - \sigma_1} \quad (16)$$

$$\text{Width at the blade entrance } (b_1), \text{ considering } \sigma 1,\ b_1 = \frac{Q'}{v_{\mathrm{m1}}(\pi d_{\mathrm{m1}} - Z\sigma_1)} \quad (17)$$

$$\text{Peripheral speed at output } (u_2),\ u_2 = k_{\mathrm{u2}}\sqrt{2gH} \quad (18)$$

$$\text{Impeller output diameter } (d_2),\ d_2 = \frac{60\ u_2}{\pi n} \quad (19)$$

$$\text{Desired height (He) for } \varepsilon = 0.87,\ He = \frac{H}{\varepsilon} \quad (20)$$

$$\text{Lifting height (H}'\text{e), adopting : } \psi \text{ from 1.1 to 1.2, } H'e = He\left(1 + \frac{8}{3} \times \frac{\psi}{Z}\right) \quad (21)$$

$$\text{Southern speed at the impeller outlet } (v_{\mathrm{m2}}),\ v_{\mathrm{m2}} = k_{\nu m2}\sqrt{2gH} \quad (22)$$

$$\text{Peripheral speed at impeller outlet } \left(u_{2(\mathrm{corr})}\right),\ u_{2(corr)} = \frac{v_{\mathrm{m2}}}{2\ \tan\beta_2} + \sqrt{\left(\frac{v_{\mathrm{m2}}}{2}\frac{1}{\tan\beta_2}\right)^2 + gH'_2} \quad (23)$$

$$\text{Reed output diameter of impeller } \left(d_{2(ret)}\right),\ d_{2(ret)} = \frac{60\ u_{2\ (corr)}}{\pi n} \quad (24)$$

$$\text{Circumferential pitch between blades } (t_2),\ t_2 = \frac{\pi d_{2(ret)}}{Z} \quad (25)$$

$$\text{Impeller blade thickness } (S_1 = S_2) \quad \begin{matrix} \text{3 to 4 mm se : } d_2 < 30\ \text{cm; ou;} \\ \text{5 to 7 mm se : } 30\text{cm} > d_2 > 50\text{cm} \end{matrix} \quad (26)$$

$$\text{Obstruction due to blade thickness at outlet } (\sigma_2),\ \sigma_2 = \frac{S_2}{Sen\beta_2} \quad (27)$$

$$\text{Coefficient of contraction } (\gamma_2),\ \gamma_2 = \frac{t_2 - \sigma_2}{t_2} \quad (28)$$

$$\text{Rectified blade width } \left(b_{2(ret)}\right),\ b_{2(ret)} = \frac{Q'}{\pi d_{2(ret)} v_{\mathrm{m2}} \gamma_2} \quad (29)$$

To better demonstrate, it is important to understand the velocity triangles considered in the pumping process [13, 14]. Carvalho [15] reports that knowing these speeds is critical to any flow machine design (hydraulic turbines, gas turbines, fans, rotary compressors, hydraulic pumps, etc.).

Finally, the algorithm provides the constructive characteristics that were used to calculate the forces acting on the impeller blades. Based on the rotation variation of

the impeller of 100, 95, 90, 85, and 80%, maintaining the specific rotation (nq) and flow (Q) constant, it was possible to calculate the variation of the rotation of the impeller [9].

3.1 Determination of forces on impeller blades

Based on the constructive characteristics of the impeller, the length of the blade was determined, which, in turn, was divided into five sections to determine the acting forces (**Figure 3**).

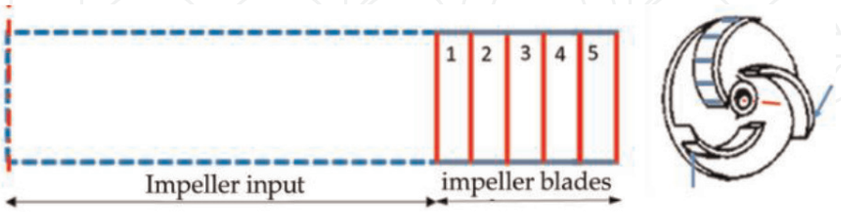

Figure 3.
Diagram of division of impeller blade sections.

Based on the velocity fields that occur in each section of the impeller blade, the abrasive drag forces occurring on the blade surface were determined. According to Fox [16], drag is the component of force on a body that acts parallel to the direction of relative motion and can be written as presented in Eq. (30).

$$F_D = \frac{Cd\rho V^2 A}{2} \tag{30}$$

Considering that the flow is initially laminar and in the course of the flow area, it becomes turbulent, the drag coefficient can be calculated by Eq. (31).

$$C_D = \frac{0.0742}{\mathrm{Re}^{(0.2)}} - \frac{1740}{\mathrm{Re}} \tag{31}$$

Fox [16] also reports that in the case of "$5 \times 10^5 < \mathrm{Re} < 10^9$", the same adjustment performed in Eq. (31) can be applied to Eq. (32) given by Schlichting in 1979, obtaining Eq. (33):

$$C_D = \frac{0.455}{(\log \mathrm{Re})^{2.58}} \tag{32}$$

Staying like this:

$$C_D = \frac{0.455}{(\log \mathrm{Re})^{2.58}} - \frac{1740}{\mathrm{Re}} \tag{33}$$

The Reynolds number (Re) is a relation between forces of inertia and viscous force, which can be expressed according to Eq. (34):

$$\mathrm{Re} = \frac{dV}{\nu} \tag{34}$$

3.2 Tests of resistance to abrasive wear

In this test, the sample was pressed by loading an inoperative weight against a rotating steel ball. The abrasive slurry was dripped onto the wear interface. After

the sphere travels through a previously established distance, called a running distance, a circular depression or crater of wear occurs on the surface of the sample [9, 10, 17–21]. **Figure 4** shows a schematic diagram of the microabrasion test device.

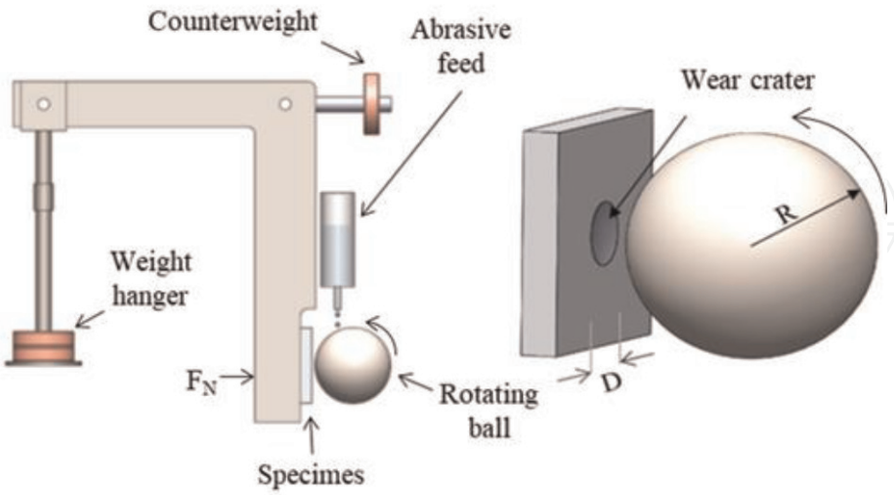

Figure 4.
Schematic diagram of the microabrasion test device.

The equations for calculating the wear coefficient from the volume of material removed in tests with spherical body were initially established by Kassman et al. [22]. Rutherford and Hutchings [23] generalized these equations for the case of flat and curved samples and for calculating the coefficient of wear of films independently of the substrate.

After the wear tests, the simplest technique for the calculation of the wear coefficient is based on the reading of the average diameter of the crater formed by the wear followed by the application of Eqs. (35)–(37) presented below [9, 10, 17, 18, 20, 21]. The diameter measurement should be performed by scanning electron microscope (SEM).

$$\text{Theoretical volume removed } (V_{TW}),\ V_{TW} = \frac{\pi D^4}{64.R} \tag{35}$$

$$\text{Wear rate } (Q_T),\ Q_T = \frac{V_{TW}}{S} \tag{36}$$

$$\text{Coefficient of material wear } (K),\ K = \frac{Q_T}{FN} \tag{37}$$

Studies suggest the application of the following test parameters: 25.4 mm diameter test sphere made of SAE 52100 steel; rotation of 100 rpm; duration of 23 minutes for each trial; scroll distance of 180 m; and FN = 3 N [9, 10].

3.3 Acquisition and preparation of analyzed samples

Of the three types of materials used in impeller manufacture (**Figure 5**), only nodular cast iron (NCI) was removed from a genuine impeller of a Flygt pump. The other samples were acquired in bar format with specifications similar to those used in the manufacture of impellers.

The samples were sanded, polished, and cleaned. For this work, the technique of manual sanding was chosen, where the samples were sanded with granulometry ranging from 100# to 1200#, changing the direction by 90° in each change of

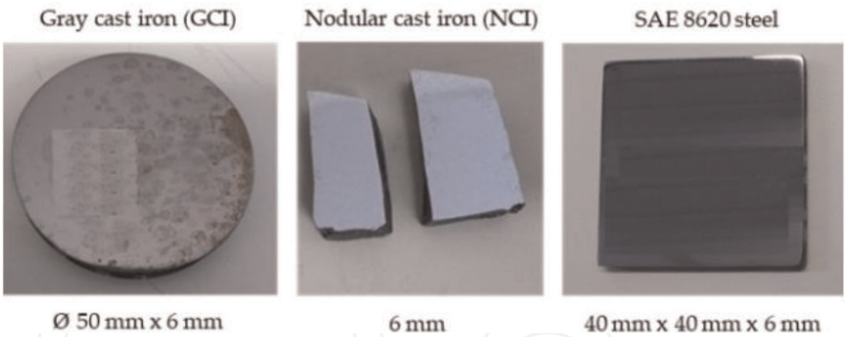

Figure 5.
Samples analyzed in the abrasion tests.

sandpaper, being careful to change the sandpaper only when the traces of the previous sandpaper did not appear (**Figure 6**) [24].

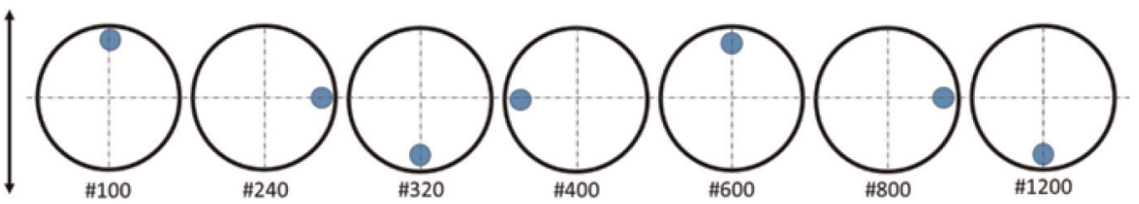

Figure 6.
Schematic representation of the sanding method.

After sanding, the samples were subjected to a 1-μm alumina polishing procedure at a concentration of 10%, followed by polishing with a 1-μm diamond paste and 0.25 μm for a nonmarking surface finish (**Figure 7**).

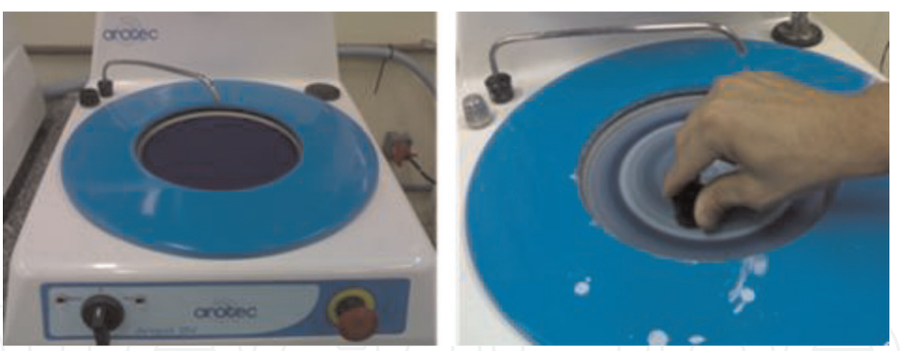

Figure 7.
Polishing the sample in bench polisher.

The samples were then washed in tap water to remove traces of the abrasives, followed by the application of ethyl alcohol to facilitate drying.

3.4 Preparation of abrasives

Each sediment sample was shaken with distilled water for homogenization in five different concentrations 0.1, 0.2, 0.3, 0.5, and 1.0% (1, 2, 3, 5, and 10 g L^{-1}, respectively) (**Figure 8**).

To compare the abrasiveness of the sediments and the abrasive wear resistance of test bodies, a 1% concentration (10 g L^{-1}) abrasive suspension of silicon carbide (SiC) was also prepared (**Figure 9**). This procedure allows to record a reference abrasiveness caused by the sediment used in comparison of a standard abrasive, commonly used in other tests [9, 10].

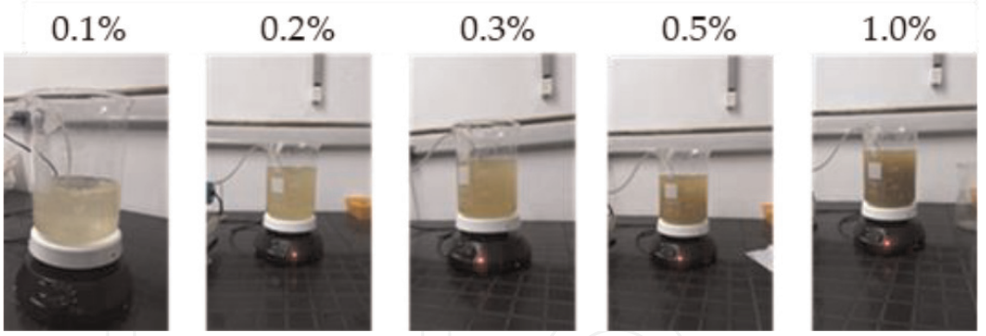

Figure 8.
Preparation of abrasive suspensions with Acre River sediments.

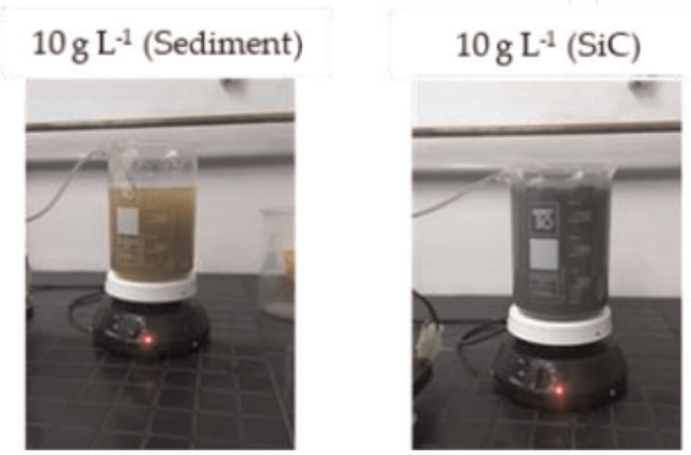

Figure 9.
Preparation of abrasive solutions (sediment and SiC).

To obtain the granulometric distribution of sediment particles, the combined analysis of the sedimentation and sieving method was used [25].

3.5 Impulse wear estimate

The estimated wear of the impeller blades was predicted based on the modified Archard equation [20], where the coefficient of wear (k) presented in Eq. (1) is a dimensionless constant that is divided by the hardness of the worn material (H) and that the K displayed in Eq. (37) refers to a specific wear coefficient for a material as a function of an abrasive, allowing the following adjustment (Eq. 38) [9, 10]:

$$V_{TW} = K \bullet FN \bullet S \tag{38}$$

Considering the relative velocity of the mixture (water + sediment) passing through a certain area of the impeller blade, a relative distance (S) was estimated according to Eq. (39) [9, 10]. The FN force considered in this analysis was calculated from Eq. (30) of the drag force occurring in a particular section of the blade.

$$S = V \bullet t \tag{39}$$

Based on the variation of the Acre River account [26], which changes manometer height (H) of the GWES, wear was determined as a function of the variation of the pump rotation in 100, 95, 90, 85, and 80%, due to the variation of the head (ΔH), maintaining the volume of water pumped. The reduction of the FD due to the reduction of the relative speed (w), due to the reduction of the rotation of the

pump, to estimate the variation of the wear of the impeller blades due to the variation of the sediment load and the Acre river quota was observed.

4. Results and discussion

4.1 Impeller characteristics

To determine the characteristics of the impeller, consideration was given to the need of GWES of the water treatment station II (WTS II), which works with pumps with flow of 1080 $m^3\ h^{-1}$ (300 L s^{-1}) driven by an electric motor with rotation of 1180 rpm and a head of 25 m (considering hydraulic losses). The results can be seen in **Table 1** and **Figure 10**.

Based on **Table 1**, the propeller length of 140.2 and 7 mm thickness was determined (**Figure 10A** and **B**). The impeller blade has been divided into five sections to determine the abrasive drag forces (**Figure 10C**), which vary from inlet to outlet inlet.

Then, five conditions were simulated, where the flow (Q), the specific rotation (nq), was maintained to relate the rotation (n) of the pump (80, 85, 90, 95 and 100% of 1180 rpm), as a function of the variation of the head (ΔH) Acre (**Figure 11**).

Impeller characteristics	
Diameter of impeller inlet (d1)	312 mm
Impeller outlet diameter (d2)	408 mm
Angle of blade at impeller inlet (β1)	17.45°
Angle of blade at impeller outlet (β2)	23°
Blade width at impeller inlet (b1)	99 mm
Width of blade at impeller outlet (b2)	63 mm
Thickness of impeller blades	6 mm
Number of impeller blades	7
Southern speed at impeller inlet (vm1)	4.89 m s^{-1}
Southern speed at impeller outlet (vm2)	4.27 m s^{-1}
Peripheral velocity at impeller inlet (u1)	15.57 m s^{-1}
Peripheral speed at impeller outlet (u2)	25.18 m s^{-1}
Relative speed at impeller inlet (w1)	16.31 m s^{-1}
Relative speed at impeller outlet (w2)	10.94 m s^{-1}

Table 1.
Constructive characteristics calculated.

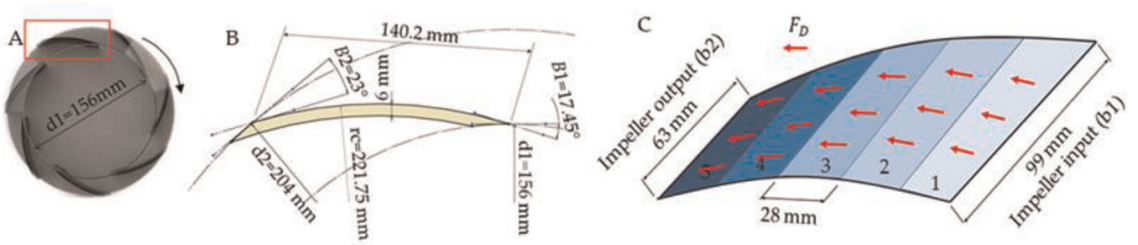

Figure 10.
Determination of the five sections of the impeller blade to determine the abrasive drag forces on the blade surface.

4.2 Determination of forces applied to impeller blades

As shown in **Figure 10** and applying Eq. (30) and the variation of the relative speed (w) shown in **Figure 11**, the abrasive drag force (FD), which varies as a function of the impeller radius in each section of the sheet, is calculated. In this way, it can be observed that the FD is larger in Section 2, with a tendency to decrease toward the exit of the impeller blades (**Figure 12**).

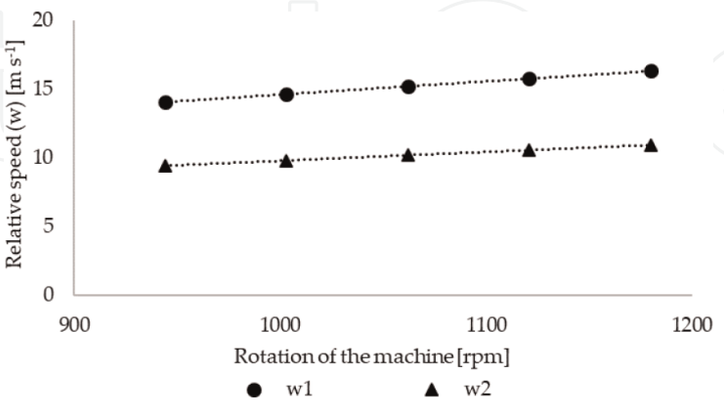

Figure 11.
Variation of the relative speed (w) in the impeller blade, due to the variation of the pump rotation: w1 inlet and w2 outlet.

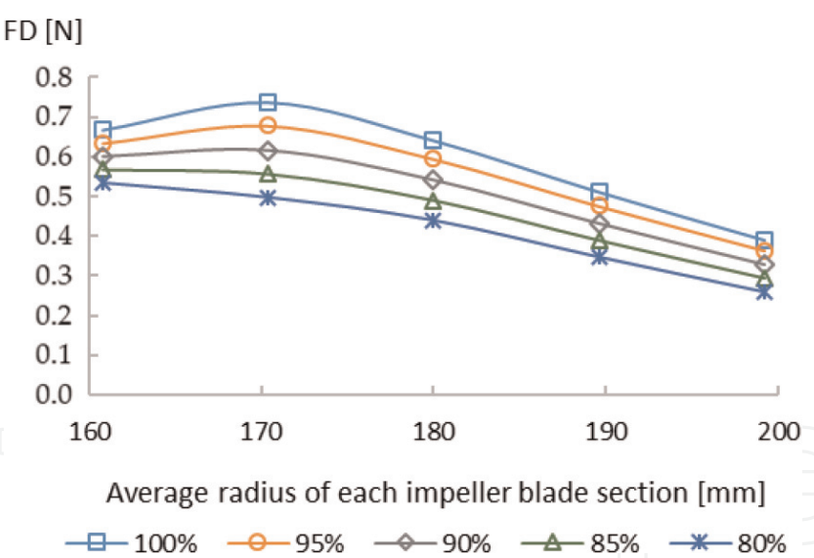

Figure 12.
Variation of the FD to the radius of each section of the impeller blade and the rotation variation from 80 (944 rpm) to 100% (1180 rpm).

4.3 Analysis of the erosive sediments of Acre River

The particles pumped by the impellers may show differences of granulometry and concentration due to the effect of turbulence at the entrance of the uptake ducts of said elevation stations, due to the slight dredging effect. In the case of the samples collected in the desanding tank, after the pumping, they presented a concentration of 60% of the sediment load with granulometry varying from 0.075 to 0.420 mm, with 1.36% having a granulometry greater than 0.420 mm and the remaining 40.35% with particle size below 0.075 mm diameter D50 of 0.097 mm (**Figure 13**).

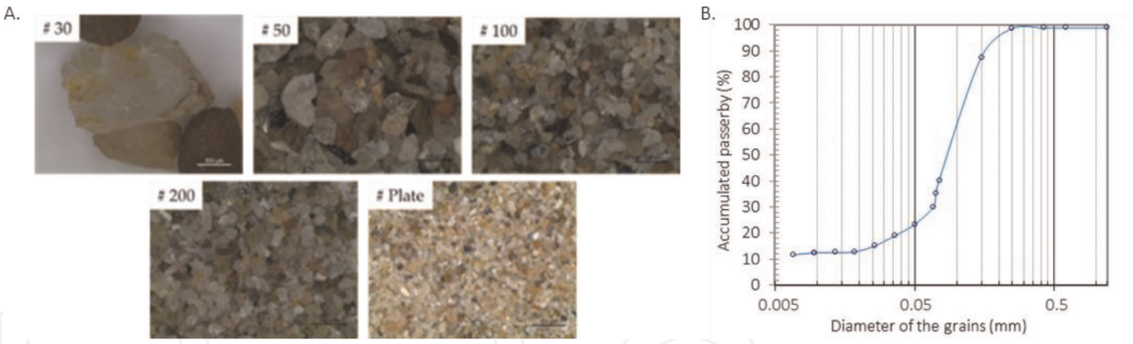

Figure 13.
Classified morphology of the erosive sediments present in the waters of the Acre River, collected from the WTS II degrading tank.

The sediments presented granulometric classification of very fine to fine sand [27] or simply sand [28]. According to visual interpretation, sediment grains are classified as semiround to semiround, characteristic of young and sandy soils. These characteristics indicate a high abrasive power due to the sharp tips and the large quantity of quartz grains with a hardness of 4–6 on the Mohs scale.

4.4 Rotating ball abrasion tests and crater analysis

From the diameters of the craters generated in the wear tests for the sediment concentrations analyzed, the coefficient of wear (K) was calculated from Eq. (37).

To analyze the relationship of K as a function of the concentration of sediment in the abrasive suspension, for each of the analyzed materials, logarithmic curves were drawn (**Figure 14**). The values of K at the concentration of 0.5 g L^{-1} were calculated by the curve equation, generated experimentally for the concentrations of 1, 2, 3, 5, and 10 g L^{-1}. Thus, it was observed that K increased as a function of the increase of the sediment concentration, for FN = 3N, probably due to the higher amount of abrasive particles in contact between the sample and the sphere, resulting in higher wear [9, 10, 21, 29–32].

It is also observed that the increase of K does not present a linear proportion with the increase of the concentration, considering that not all the particles of the abrasive suspension can come into contact with the worn surface, corroborating with that described by Hutchings and Shipway [33].

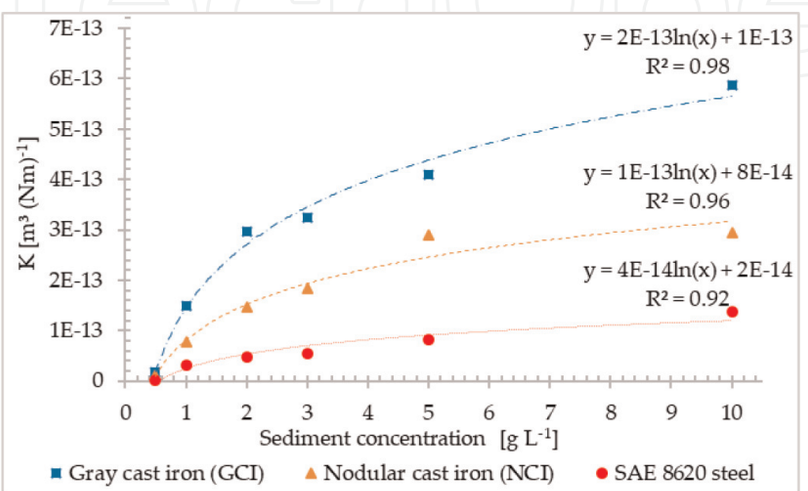

Figure 14.
Behavior of the specific wear coefficient (K) due to the sediment concentration variation, for the test conditions (S = 180 m and FN = 3N).

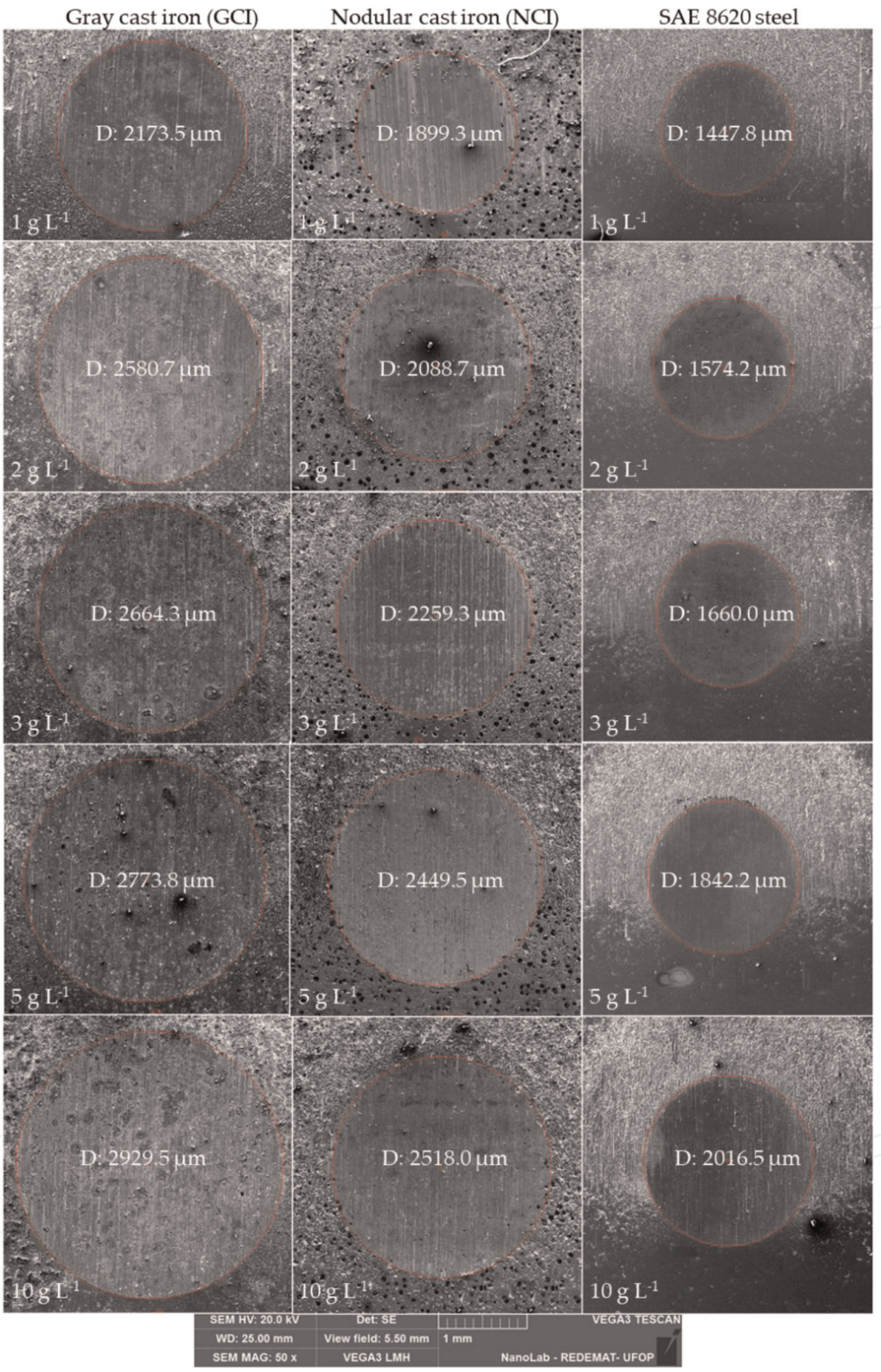

Figure 15.
Influence of sediment concentration on the diameter of the wear cap (SEM).

Figure 15 shows the wear evolution due to the sediment concentration, as well as the difference in crater diameter, for each test specimen used. At the outset, it is possible to observe the presence of wear grooves characteristic of abrasive tests.

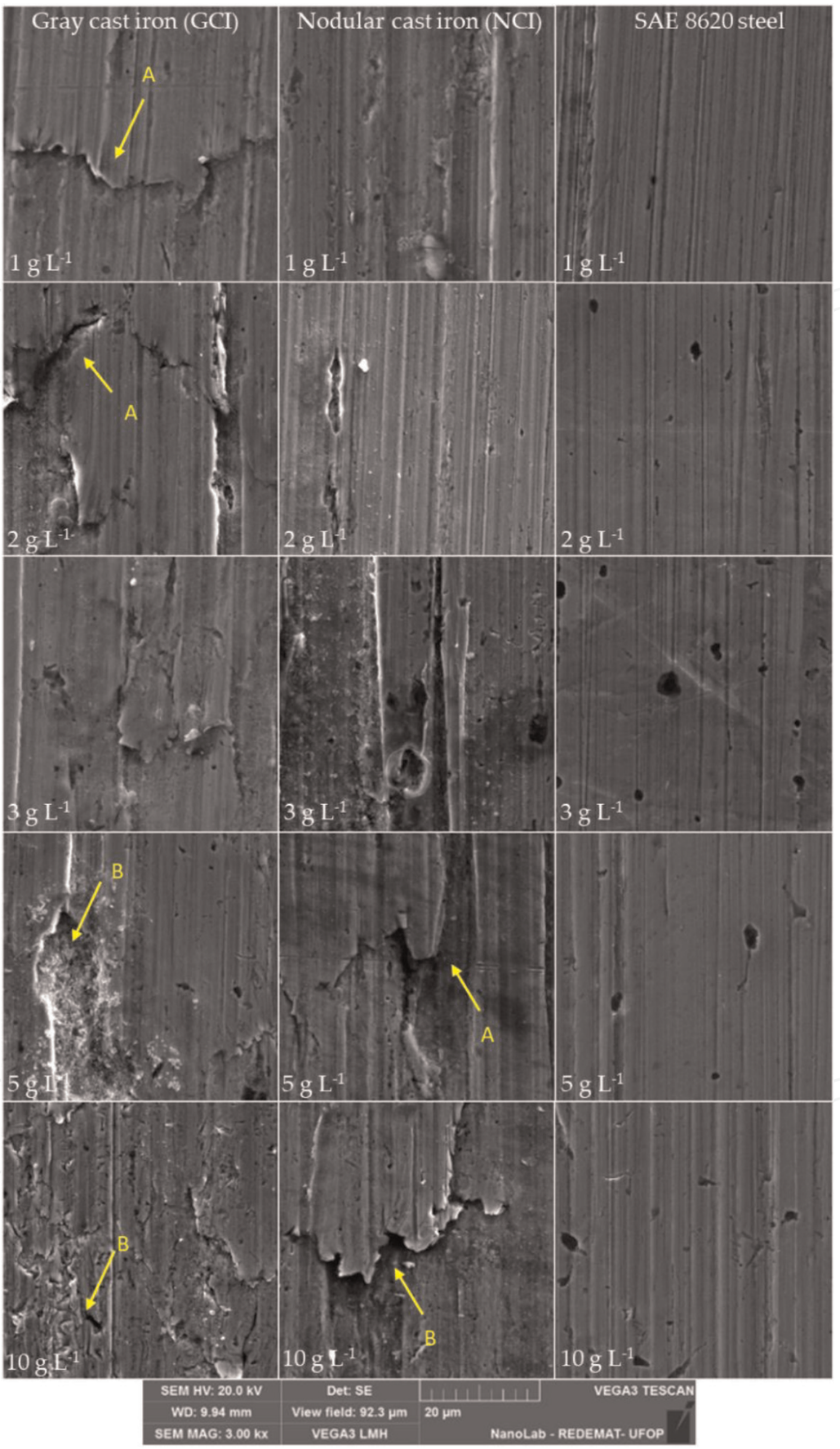

Figure 16.
Evaluation of the wear pattern as a function of sediment concentration (SEM): (A) plastic deformation and (B) tipping points of that of the accumulations in front of the grooves.

From what is shown in **Figure 16**, it can be observed that the wear pattern did not change as a function of the sediment concentration, maintaining the wear pattern by grooving for the three metal alloys, with a clear orientation. These results also reflect features similar to the wear pattern found by Cozza [34] and Serrano et al. [9], referring to concentrations of abrasive less than 18% and a load greater than 1N.

In addition, it is observed in **Figures 15** and **16** that the GCI and NCI specimens presented areas with clear plastic deformations (A), with intensification as a function of the increase in sediment concentration, with a clear accumulation of material at the front of the wear grooves and with greater intensity of deformation in the GCI. The materials accumulated at the edges of the grooves are later removed by the association of the microstructural mechanisms with the mechanism of low cycle fatigue (B), similar to that observed by Serrano et al. and Pintaúde [9, 10, 31].

The average volume of waste material caused by the sediment was 340% higher, compared to the wear caused by the SiC. The results can be explained by the granulometric difference of the abrasive materials, where the sediment particles presented D50 six times larger than the SiC particles, 0.097 and 0.016 mm, respectively. Considering the homogeneity of SiC hardness and grain size, it will allow the comparison of the wear intensity caused by sediments from different river basins [9].

4.5 Determination of blade wear

Considering the relative velocities at the inlet and outlet of the impeller (**Figure 11**), the variation of FD on the blades (**Figure 12**) and the variation of K as a function of the sediment load (**Figure 14**) were applied to Eq. (38) to estimate the paddle wear volume, due to the variation of the sediment load and the monthly mean level of the Acre River (**Figure 17**).

As shown in **Figure 17**, the nonapplication of the rotational control of the machine, taking advantage of the reduction of the ΔH as a function of the increase of the river's elevation, can lead to premature wear of the impeller due to the increase of the sediment concentration carried by river, the during the rainy season.

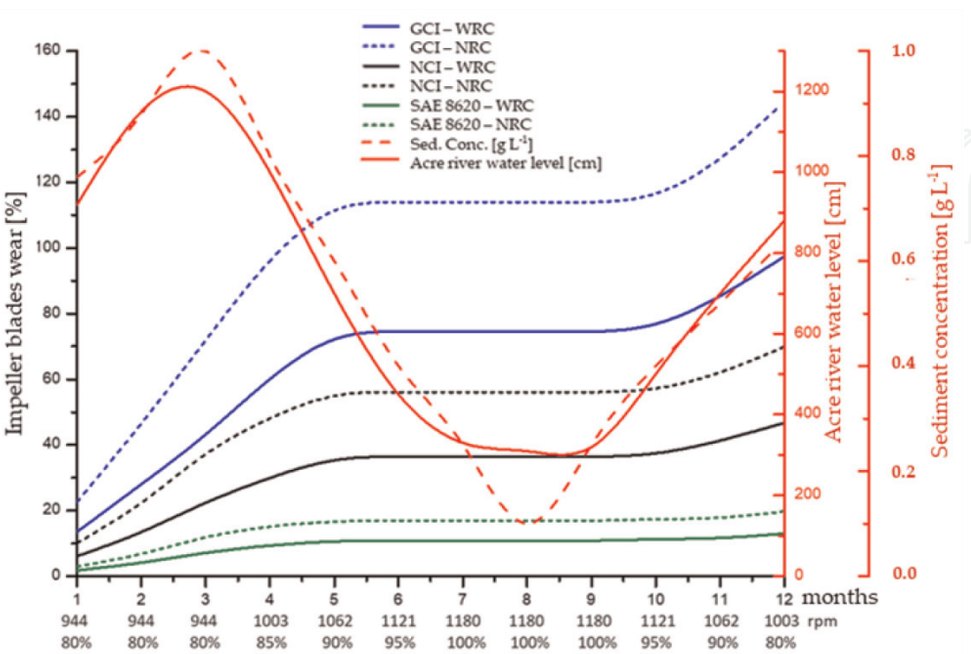

Figure 17.
Accumulated wear of the impeller blade, due to the variation of the sediment concentration of the Acre River: with rotational control (WRC) and without rotational control (NRC).

In the case of the study presented here, when applying rotational control, the relative velocity of the fluid decreased, reducing the FD on the impeller blades, also reducing the wear.

When looking at the wear accumulated in **Figure 17** and considering the wear limit at 70% of the thickness of the impeller blades, it can be concluded that without the rotational control, it would require two GCI impellers per year or one NCI impeller, while the SAE 8620 steel impeller could run for almost 3 years. Already with the rotational control, this wear can be reduced by approximately 33%.

Also in **Figure 17**, the higher resistance of SAE 8620 steel can be verified, being 7.3 times more resistant than GCI and 3.5 times more resistant than NCI, whereas NCI is 2 times more resistant than the GCI.

5. Conclusions

The abrasive wear regime and the reproducibility of the results under the test conditions in the present work were adequate to investigate the abrasive capacity of the sediments and the wear of GCI, NCI, and ASE 8620 steel.

The semiangle and semirounded forms of the Acre River sediments produced evidence of microstrip and plastic deformation of the material in the three metal alloys at all sediment concentrations used in the tests.

The analysis of the wear volume, according to the type of metal alloy, the sediment concentration, and the relative velocity in the impeller blades, showed the importance of a previous study of the sediment concentration in the water sources pumped by GWES, as well as ΔH and the required flow rate, to select the material used to make the impeller.

The analysis of the variation of the impeller rotation as a function of the river level variation and the variation of the head (ΔH) showed the possibility of reducing the impeller wear by up to 30% in a hydrological cycle for the three metal alloys used in the tests, showing the importance of rotational control during the pumping process.

Considering that the three metal alloys presented the same percentages of wear reduction as a function of the rotational control, maintaining the same volume of water pumped, it is suggested that such control can be adopted in GWES from other locations that show load variation of sediment and fluviometric dimension.

Acknowledgements

The authors are grateful for the financial support: Gorceix Foundation; CEMIG; ANEEL; FAPEPIG; ELETROBRAS-FURNAS; CAPES; and CNPq.

They also thank the Laboratory of Thermal Treatment and Optical Microscopy (LTM), the Laboratory of Electron Microscopy (NanoLab), the Laboratory of Microabrasive Foundry and Wear of UFOP, the Center for Hydraulic Research and Water Resources (CPH) of UFMG, and the Laboratory of Geomorphology and Sedimentology of UFAC, for technical and experimental support.

Nomenclature

V_W	volume of material removed (m^3)
k	coefficient of wear (dimensionless)
Hm	hardness of material (N mm^{-2})
FN	normal force applied (N)

S	sliding distance (m)
nq	specific rotation (rpm)
n	impeller rotation (rpm)
Q	pump flow rate (L s^{-1})
H	manometric height (m)
Q_{gpm}	pump flow rate (gpm)
gpm	gallons per minute
ηt	absolute yield
kv'1	the coefficient of velocity at the inlet port of the impeller
g	gravitational constant (m s^{-2})
π	PI
Q'	correction pressure: due to recirculation (m^3 s^{-1})
K_{vm1}	coefficient of the velocity of the meridian component at the impeller inlet
F_D	abrasive drag force (N)
C_d	drag coefficient
ρ	fluid density (kg m^{-3})
V	fluid relative velocity (m s^{-1})
A	area (m^2)
d	length of fluid displacement (m)
ν	kinematic viscosity (m^2 s^{-1})
$\boldsymbol{D}$	wear crater diameter (m)
R	ball radius (m)
Q_T	wear rate (m^3 m^{-1})
K	specific wear coefficient (mm^3 (N m)$^{-1}$)
V_{TW}	theoretical volume removed (m^3)
t	impeller run time (s)
ΔH	variation of manometric height (m)
K_{vm2}	coefficient of velocity of the meridian velocity component at the impeller outlet

Author details

Rodrigo O.P. Serrano[1,4*], José G. do V. Moreira[2], Ana L.P. de Castro[3], Maria A. Pinto[3], Edna M. de F. Viana[4] and Carlos B. Martinez[4]

1 Federal University of Acre—UFAC, Rio Branco, Acre, Brazil

2 Federal University of Acre—UFAC, Cruzeiro do Sul, Acre, Brazil

3 Federal University of Ouro Preto—UFOP, Ouro Preto, Minas Gerais, Brazil

4 Federal University of Minas Gerais—UFMG, Program in Mechanical Engineering, Belo Horizonte, Minas Gerais, Brazil

*Address all correspondence to: ropereas@gmail.com

References

[1] Carvalho AT, Costa ML, Almeida HDF. Os Sedimentos em Suspenção dos Rios Purus e Juruá no Estado do Acre. Revista Científica da UFPA, v.7. 2008:8

[2] Serrano ROP, Ferreira-Junior AG, Castro ALP, Santos PABV, Menezes MV, Martinez CB. Desgaste do rotor por abrasão: O efeito do bombeamento de água bruta com diferentes cargas de sedimento. In: XXVII Congreso Latinoamericano de Hidráulica, AIRH. Lima, Perú; 2016. pp. 26-30

[3] Xing D, Hai-lu Z, Xin-yong W. Finite element analysis of wear for centrifugal slurry pump. In: Proceedings of the international conference on mining science and technology (ICMST). Procedia Earth and Planetary Science. 2009;**1**:1532-1538. DOI: 10.1016/j.proeps.2009.09.236

[4] Hutchings IM. Tribology: Friction and Wear of Engineering Materials. 1st ed. Londres: Edward Arnold; 1992. 273 p

[5] Upadhyay RK, Kumaraswamidhas LA. A review on tribology of surfaces and interfaces. Advanced Materials Letters. 2014;**5**(9):486-495. DOI: 10.5185/amlett.2014.5566

[6] ASTM—G40. Standard terminology relating to wear and erosion. In: G 40, Annual Book of ASTM Standards. ASTM International; 2015

[7] DIN. DIN 50320. Wear; terms, systematic analysis of wear processes, classification of wear phenomena. International Classification for Standards. Alemannic; 1979. 8 p

[8] Archard JF, Hirst W. The wear of metals under unlubricated conditions. Proceedings of the Royal Society. 1956; **236**:397-410. DOI: 10.1098/rspa.1956.0144

[9] Serrano ROP, Santos LP, Viana EMF, Pinto MA, Martinez CB. Case study: Effects of sediment concentration on the wear of fluvial water pump impellers on Brazil's Acre River. Wear. 2018;**408–409**:131-137. DOI: 10.1016/j.wear.2018.04.018

[10] Serrano ROP, Castro ALP, Rico EAM, Viana EMF, Pinto MA, Martinez CB. Abrasive effects of sediments on impellers of pumps used for catching raw water. Revista Brasileira de Engenharia Agrícola e Ambiental. 2018; **22**(9):591-596. DOI: 10.1590/1807-1929/agriambi.v22n9p591-596

[11] Duan CG. Approach to the demand on anti abrasive Erosion from hydraulic machinery project. Hydraulic machinery and cavitation. In: Proceedings of XIX IAHR Symposium, World Science. Singapore; 1998. pp. 59-69

[12] Serrano ROP. Metodologia para avaliação de desgaste abrasivo em pas de rotor de bombas centrifugas de estação elevatória [thesis]. Belo Horizonte, Minas Gerais, Brazil: Federal University of Minas Gerais; 2017

[13] Palomino AEC. Desenvolvimento de metodologia para determinação dimensional de uma bomba centrífuga utilizando velocidades específica [dissertation]. Bolo Horizonte, Minas Gerais, Brazil: Universidade Federal de Minas Gerais; 2017

[14] Macintyre AJ. Bombas e instalações de bombeamento. 2nd ed. Rio de Janeiro: LTC; 2013. 430 p

[15] Carvalho DF. Instalações elevatórias – Bombas. FUMARC – Fundação Mariana Resende Costa; 2010. 365 p

[16] Fox RW, McDonald AT, Pritchard PJ. Introdução à mecânica de fluidos. Tradução de Ricardo Nicolau Nassar Koury, Geraldo Augusto Campolina.

Vol. 2006. Rio de Janeiro: França, LTC; 1934. 513 p

[17] Rutherford KL, Hutchings I, Rutherford K. Theory and application of a micro-scale abrasive wear test. Journal of Testing Evaluation of the American Society for Testing and Materials. 1997;**25**(2):250-260. DOI: 10.1520/JTE11487J

[18] Allsopp DN, Hutichings IM. Micro-scale abrasion and scratch response of PVD coatings at elevated temperatures. Wear. 2001;**251**:1308-1314. DOI: 10.1016/S0043-1648(01)00755-4

[19] Cozza RC, Rodrigues LC, Schon CG. Analysis of the micro-abrasive wear behavior of an iron aluminide alloy under ambient and high-temperature conditions. Wear. 2015;**330-331**: 250-260. DOI: 10.1016/j.wear.2015.02.021

[20] Santos WC, Pereira-Neto JO, Silva RO, Rodrigues G, Moreto JÁ, Manfrinato MD, et al. Desenvolvimento de dispositivo e estudo do comportamento ao micro desgaste abrasivo do aço AISI 420 temperado e revenido. Revista Matéria. 2015;**22**(02): 304-315. DOI: 10.1590/S1517-707620150002.0031

[21] Krelling AP, Costa CE, Milan JCG, Almeida EAS. Micro-abrasive wear mechanisms of borided AISI 1020 steel. Tribology International. 2017;**111**: 234-242. DOI: 10.1016/j.triboint.2017.03.017

[22] Kassman A, Jacobson S, Erickson L, Hedenqvist P, Olsson M. A new test method for the intrinsic abrasion resistance of thin coatings. Surface and Coatings Technology. 1991;**50**:75-84. DOI: 10.1016/0257-8972(91)90196-4

[23] Rutherford KL, Hutchings IM. A micro-abrasive wear test with particular application to coated systems. Surface and Coatings Technology. 1996;**79**: 231-239. DOI: 10.1016/0257-8972(95)02461-1

[24] Rohde RA. Metalógrafia—Preparação das amostras: Uma abordagem pratica. LEMM: URI; 2010. 30 p

[25] ABNT—Associação Brasileira de Normas Técnicas. NBR 7181—Solo—Análise granulométrica—Métodos de ensaios. 1984

[26] Duarte AF, Gioda A. Inorganic compositional of suspended sediments in the Acre River, Amazon Basin, Brazil. Latin American Journal of Sedimentology and Basin Analysis. 2014;**21**(1):3-15

[27] Wentworth CK. A scale of grade and class terms for clastic sediments. Journal of Geology. 1922;**30**:377-392

[28] ABNT—Associação Brasileira de Normas Técnicas. NBR 6502—Rochas e solos. Brazil; 1995. 18 p

[29] Cozza RC. Estudo do desgaste e atrito em ensaios micro-abrasivos por esfera rotativa fixa em condições de força normal constante e pressão constante [thesis]. Escola Politécnica da USP; 2011

[30] Trezona RI, Allsopp DN, Hutchings IM. Transitions between two-body and three-body abrasive wear: Influence of test conditions in the microscale abrasive wear test. Wear. 1999;**225-229**: 205-214. DOI: 10.1016/S0043-1648(98)00358-5

[31] Pintaúde G. Análise dos regimes moderado e severo de desgaste abrasivo utilizando ensaios instrumentados de dureza [thesis]. Escola Politécnica da USP; 2002

[32] Fernandes F, Ramalho A, Loureiro A, Cavaleiro A. Mapping the micro-abrasion resistance of a Ni-based coating deposited by PTA on gray cast iron.

Wear. 2012;**298**(293):151-158. DOI: 10.1016/j.wear.2012.05.018

[33] Hutching IM, Shipway P. Tripology: Friction and Wear of Engineering Materials. 2nd ed. Butterworth Heinemann; 2017. 412 p. e-book ISBN: 9780081009512

[34] Cozza RC. Effect of pressure on abrasive wear mode transitions in micro-abrasive wear tests of WC-Co P20. Tribology International. 2013;**57**: 266-271. DOI: 10.1016/j.triboint.2012.06.028